Cells Take up and Recover from Protein-Stabilized Single-Wall Carbon Nanotubes with Two Distinct Rates

Brian D. Holt,[†] Kris Noel Dahl,[†,‡,*] and Mohammad F. Islam[§,*]

[†]Department of Biomedical Engineering, [‡]Department of Chemical Engineering, and [§]Department of Materials Science & Engineering, Carnegie Mellon University, 5000 Forbes Avenue, Pittsburgh, Pennsylvania 15213-3890, United States

ABSTRACT

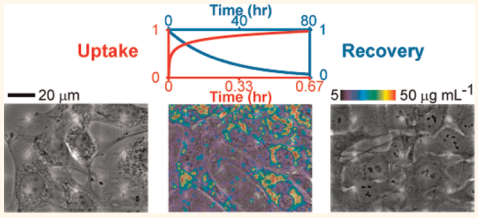

Single-wall carbon nanotubes (SWCNTs) are increasingly being investigated for use in biomedical applications for intracellular imaging and ablation, as well as vehicles for drug and gene delivery. One major obstacle to the development of safe, controlled, and effective SWCNT-based biomedical materials is limited quantification of dosage- and time-dependent uptake kinetics, cellular effects, and recovery profiles. Here, we quantified NIH-3T3 cellular uptake of and recovery from individualized SWCNTs dispersed using a biocompatible dispersing agent, bovine serum albumin (BSA). Uptake and recovery were determined by monitoring the mass of SWCNTs-BSA per cell, as a function of SWCNTs-BSA over the concentration range of 1 to 100 μg mL^{-1} and time range of seconds to days. To determine SWCNTs-BSA biocompatibility as a function of uptake and recovery, cytotoxicity, proliferation potential, and cell phenotype were monitored for each condition. Interestingly, the rate of cellular uptake of SWCNTs-BSA was rapid, reaching steady state within ~1 min, in agreement with modeling. We also observed a threshold SWCNT exposure level (>1 μg mL^{-1}) above which internalization is saturated and uptake scales linearly with exposure amount. Cells were able to recover from SWCNTs-BSA over ~30 h, regardless of dosage level or exposure time. We suggest that these differential rates of uptake and recovery, quantified in our work, may enable cell-based SWCNT delivery systems.

KEYWORDS: carbon nanotube · uptake · recovery · NIH-3T3 cells · bovine serum albumin

Development of single-wall carbon nanotube (SWCNT)-based cellular technologies requires advances in multiple fronts, such as generation of biocompatible SWCNTs that are not toxic, do not illicit an immune response, and do not interfere with normal cell processes, while maintaining the inherent properties of SWCNTs. Initially, nonpurified, bundled, and long SWCNTs had been associated with toxicity and negative cellular effects.[1−4] Purification of SWCNTs to remove catalyst and carbonaceous impurities,[5,6] dispersion into isolated tubes using biocompatible agents,[3,7−22] and selection of short (100s of nm) SWCNTs for optimal cellular delivery[23] has produced nontoxic SWCNTs appropriate for biological applications. These biocompatible SWCNTs have been utilized as drug delivery platforms,[9] showing promising results *in vitro* specifically for anticancer drug[8,24−29] and nucleic acid[30−32] delivery inside the cell. Other studies have shown that SWCNTs enter cells *via* endocytosis[4,13,19,20,33−35] and localize within different compartments of the cell.[7,36−39] SWCNTs, visualized directly by Raman spectroscopy[2,4,7,8,20,35,36,38,40,41] and near-infrared (NIR) fluorescence microscopy[19,21,22,37,42] or *via* fluorescent conjugation,[24,29,39,42−47] can remain in cells for months with little deleterious effects.[38]

Examination of the time- and concentration-dependent rates of SWCNT uptake and an ability of cells to recover from SWCNT exposure, albeit over a limited range of dosage level and exposure time, has provided insight into cell−SWCNT interactions. Uptake and recovery has been investigated for SWCNTs coated with Pluronic F108, a bioinert polymer, with murine macrophages at low SWCNT concentrations of ≤8 μg mL^{-1} between 1 and 24 h using fluorescence spectroscopy.[21] Single-particle tracking using SWCNT fluorescence[34] has been used to determine the uptake of individual SWCNTs coated with DNA for single or double pulsed exposure with pulse widths typically on the order of minutes.[19,20]

In this paper, we report uptake rates for bovine serum albumin (BSA)-stabilized SWCNTs[7] over two decades in SWCNT concentration and multiple decades of exposure time. We quantified SWCNT concentration in cells using Raman spectroscopy,

* Address correspondence to krisdahl@cmu.edu; mohammad@cmu.edu.

Received for review February 3, 2012 and accepted March 29, 2012.

Published online March 29, 2012
10.1021/nn300504x

which identifies all SWCNTs in a linear regime. We show *via* experiment and an analytic model that SWCNTs-BSA reach steady-state internalization in one minute and that there is a threshold value of external concentration above which cellular uptake machinery is saturated. We also quantified the time- and concentration-dependent recovery rates from SWCNT exposure, showing that cells expel SWCNTs-BSA within days and recover cellular functions.

RESULTS AND DISCUSSION

Short-Time Rates of SWCNT Uptake. To determine the time-dependent uptake of SWCNTs-BSA, we first estimated the time scale for internalization *via* modeling. Previous investigations of the endocytosis and exocytosis of individual SWCNTs-DNA presented models with parameters of internalization and expulsion for pulses of SWCNTs-DNA exposure.[19,20] We used a simplified analytic model using these parameters from the pulsed exposure system for our system of continuous exposure to SWCNTs-BSA. Since cell uptake of SWCNTs occurs *via* endocytosis for SWCNTs with all dispersants examined thus far,[4,13,33] we hypothesized that rates of internalization would be cell-dependent but independent of dispersant type. Our model suggests that internalization occurs rapidly, with steady state being reached in ~1 min (Figure 1A).

Focusing on this time scale, we then designed experiments to determine time- and concentration-dependent uptake of SWCNTs-BSA by NIH-3T3 cells for exposure times ranging from 5 s to 40 min at concentrations of 1, 30, and 100 μg mL^{-1}. We quantified SWCNTs-BSA uptake using Raman spectroscopy; calibration curves show linear Raman intensity over the experimental SWCNTs-BSA concentration range (Supporting Information, Figure 1). Our experimental measurements agree with our model and show that the mass of SWCNTs-BSA per cell rapidly reached a steady state within ~1 min (Figure 1B). Previous studies of SWCNTs-DNA show experimental steady state at ≤30 min[20] or ~2 h.[19] SWCNT uptake with BSA as a dispersing agent may be more rapid than negatively charged DNA due to charge differences (possibly Columbic repulsion) and possible cell-surface receptor interaction. We also observed an order of magnitude higher SWCNTs-BSA uptake (intracellular levels compared with extracellular treatment levels) than SWCNTs-DNA.[19,20] Thus, the BSA coating on SWCNTs increases the kinetics and steady-state levels of SWCNTs by more than an order of magnitude over DNA coating.

To obtain parameters useful for designing potential SWCNT-based biotechnologies, we used the forward finite difference operator to calculate the time-dependent uptake rate for each concentration (Figure 1C). At very short times (seconds), there is a positive internalization rate, in general agreement

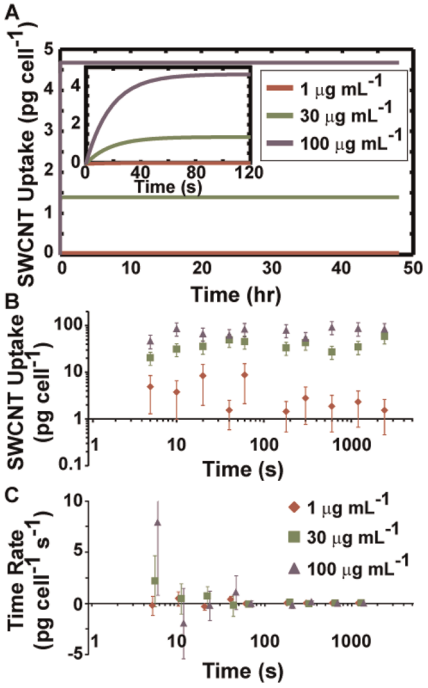

Figure 1. Concentration-dependent uptake of SWCNTs-BSA at short time. (a) Analytic solutions of endocytosis models with parameters from previously reported data[19] demonstrated rapid uptake, reaching steady state in ~1 min. (b) Experimentally determined uptake of SWCNTs-BSA into NIH-3T3 cells confirmed that a steady level of internalization was rapidly reached for different concentrations. (c) The rate of SWCNTs-BSA uptake, calculated from uptake data, showed a positive rate at very early time (<10 s), followed by oscillations, and zero at longer time.

with the model's predictions. From 10 to 100 s, there appears to be damped oscillations in the uptake rate, but sample acquisition rates were insufficient to satisfy the Nyquest theorem to determine potential higher frequency components.[48] These rates confirmed that there is no net uptake after ~1 min. The steady state was established possibly due to a balance between endocytosis and exocytosis of SWCNTs-BSA; we note that similar behavior was also observed for SWCNTs-DNA.[20]

Long-Time Rates of SWCNT Uptake. Although short-time results showed steady-state SWCNTs-BSA internalization within 1 min, cellular changes have been observed by us[3] and others[1] for substantially longer times, likely related to the time scale of cellular processes. Therefore, we performed internalization experiments with exposure times between 1 and 48 h. In agreement with the short-time results, the overall internalization of SWCNTs-BSA per cell remained constant, even after 48 h of continual exposure (Figure 2A, B).

By completely removing the SWCNTs-BSA-containing media (Figure 2B, D, F) or by performing a vigorous phosphate-buffered saline (PBS) wash step (Figure 2A, C, E), we observed changes in uptake amount but not uptake rate. The wash step significantly reduced

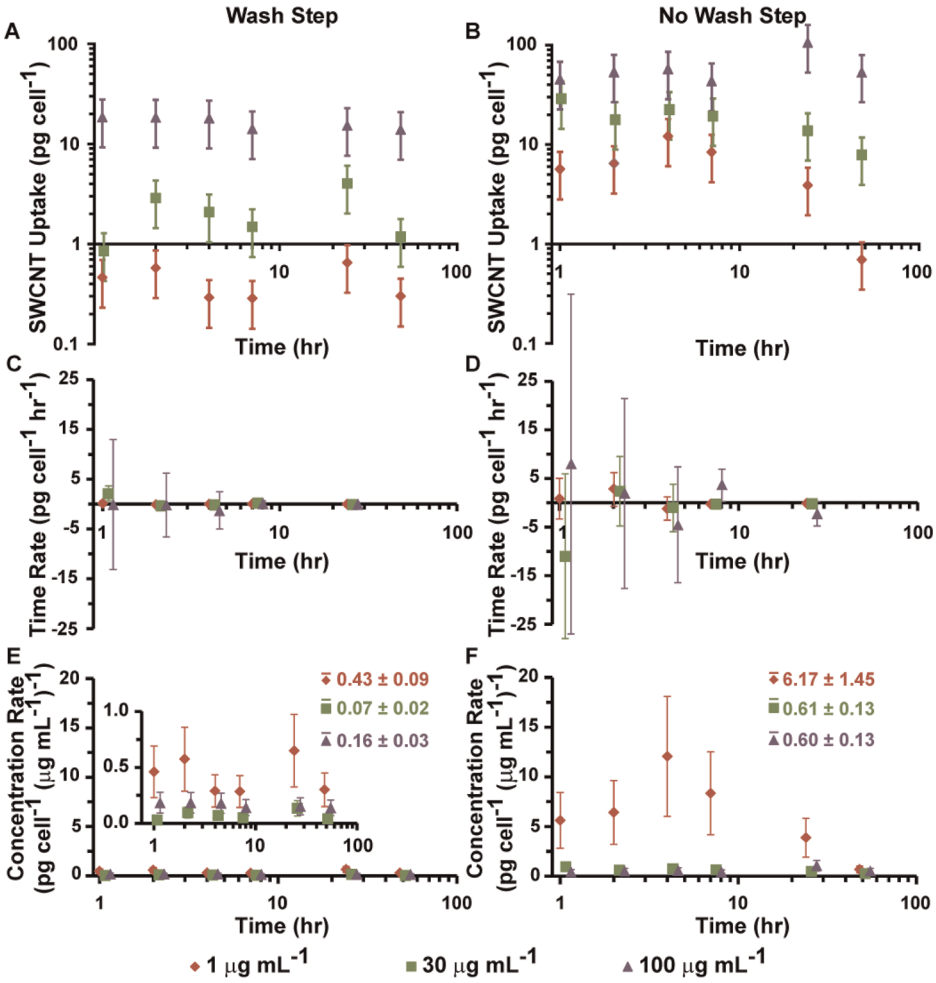

Figure 2. Concentration-dependent uptake of SWCNTs-BSA at long time. (a) SWCNTs-BSA internalization was quantified for cells with a PBS wash step prior to analysis. (b) Without the supplemental wash step, more SWCNTs-BSA were observed with cells, likely from weak membrane association. Time-dependent rates of SWCNTs-BSA uptake showed little change per time or concentration with (c) or without (d) a wash step. (e and f) Concentration-dependent rates of uptake are shown per time point per concentration. The average per concentration across all time is reported in the figure. While 30 and 100 μg mL^{-1} have similar coefficients, 1 μg mL^{-1} is strikingly higher, potentially due to a higher ratio of membrane to fully internalized SWCNTs.

(ANOVA, $p < 0.005$) the amount of SWCNTs-BSA associated with cells at each concentration. Since we have previously shown that SWCNTs associate with cell membranes,[4] we attribute this differential mass of SWCNTs to be associated with the cell membrane and, to a smaller degree, the substrate. While it is possible that agitation during the wash step may have removed cells with extremely high levels of SWCNTs that were consequently weakly attached to the substrate, we find this to be unlikely since Raman imaging of cells showed a homogeneous distribution of SWCNTs, as discussed later. We suggest that the significant mass of SWCNTs associated with the cell membrane allows fast steady-state internalization of SWCNTs-BSA by reducing diffusion limitations *via* reduction of dimensionality.

To determine the long-time parameters of internalization, finite difference operations were performed. As expected from the short-time results, the time-dependent uptake rates are 0 at long times (Figure 2C, D). Concentration-dependent internalization rates were determined by dividing the internalized SWCNT mass per cell by the external SWCNT concentration. Average concentration rates are similar for both 30 and 100 μg mL^{-1} exposures (~0.1 and ~0.6 (pg cell^{-1})/(μg mL^{-1}), for wash and no wash, respectfully). However, the concentration rate is higher for 1 μg mL^{-1} (~0.4 and ~6 (pg cell^{-1})/(μg mL^{-1}), for wash and no wash, respectfully). Since we have observed that a considerable amount of SWCNTs interact with cell membranes, it is possible that the membrane component, when exposed to 1 μg mL^{-1}, is nontrivial compared to the mass internalized. This difference in concentration rates between 1 *versus* 30 and 100 μg mL^{-1} suggests a threshold value of exposure between 1 and 30 μg mL^{-1}, below which the cell internalization machinery is not saturated and above which the machinery is saturated. As many studies investigate only low concentrations (~1 μg mL^{-1}) and potential chronic workplace exposure would occur at

low concentrations, this threshold is critical to understanding the cell response to SWCNTs at these low levels in juxtaposition to higher exposure levels, especially since the rate of internalization for subthreshold exposure levels is substantially higher than superthreshold levels.

SWCNTs-BSA Concentration-Dependent Biocompatibility. To correlate rates of SWCNT uptake with deleterious cellular effects, we determined cell viability, proliferation, and gross cellular morphology. We imaged cells with phase contrast and fluorescence microscopy, since fluorescence assays of proliferation and viability are nonlinearly quenched by SWCNTs.[1,49] We have previously found that SWCNTs influenced cells at low initial seeding density[3] ($\sim 1.5 \times 10^4$ cells cm^{-2}; 1/2 of standard seeding density).[50] These NIH-3T3 cells, seeded at low density, displayed a dose-dependent reduction in proliferation (Figure 3A) and an increase in acute cytotoxicity (Figure 3B). Cells exposed to the highest concentration of SWCNTs-BSA (*i.e.*, 100 μg mL^{-1}) essentially did not proliferate from their pre-SWCNTs-BSA levels (Supporting Information, Figure 2) and are virtually all propidium iodine (PI)-positive, indicating acute cytotoxicity. However, cells proliferated when seeded at a standard density[50] of $\sim 3.0 \times 10^4$ cells cm^{-2} (Figure 3C) and did not show SWCNTs-BSA-induced cytotoxicity (Figure 3D and Supporting Information, Figure 3). We suggest that the seeding density-dependent reduction in proliferation may be related to focal adhesions and cell spreading: cells at low seeding density, where cell–substrate interactions are more important than cell–cell interactions, may be unable to effectively spread[51] or form focal adhesions due to SWCNT-mediated actin reorganization.[3,52,53] Also, SWCNT interactions with the cell membrane may alter cell–cell signaling at low cell density. Fortunately for potential SWCNT-based biomedical devices, minimal deleterious cellular effects were observed at higher seeding densities, suggesting that SWCNTs would not be acutely cytotoxic *in vivo*.

Recovery from SWCNTs-BSA. An important consideration for SWCNT-based biomedical applications and potential workplace exposure to SWCNTs is recovery of cells after SWCNT exposure. To this end, NIH-3T3 cells were exposed to SWCNTs-BSA for 16 h at varying concentrations, were passaged, and were then either allowed to recover (*i.e.*, given fresh, SWCNTs-BSA-free media) or perpetually exposed to SWCNTs-BSA. After passage, cells were seeded at the standard density to avoid confounding low seeding density effects with an inability to recover. Cell proliferation was tracked as a function of time per experimental condition and fit with an exponential curve to obtain a proliferation time constant (τ, Figure 4A). Both recovery and perpetually exposed SWCNT samples across the range of concentrations showed no statistical change in proliferation

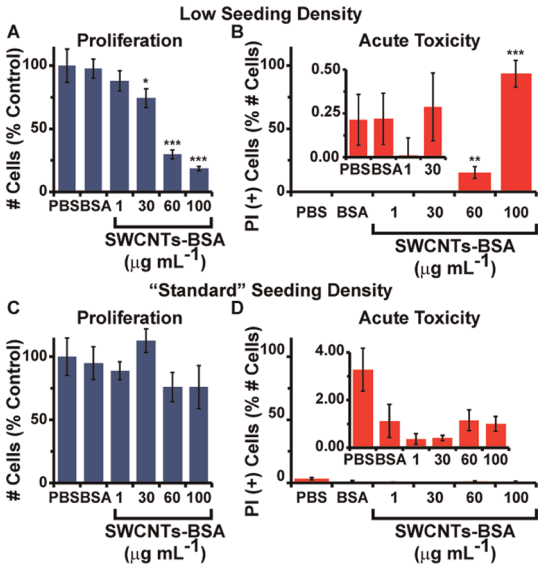

Figure 3. Biocompatibility of SWCNTs-BSA. (a) NIH-3T3 cells seeded at low density (1.5×10^4 cells cm^{-2}) showed a dose-dependent reduction in proliferation upon exposure to SWCNTs-BSA for 48 h. (b) Acute toxicity (reported by permeability to propidium iodine (PI)) showed a dose-dependent response. (c) When cells were seeded at a "standard" seeding density[50] (3.0×10^4 cells cm^{-2}), there was only a slight, nonsignificant reduction in proliferation and (d) no change in viability. Student's *t* test comparing the condition to the BSA control; *$p < 0.05$; **$p < 0.01$; ***$p < 0.0001$.

time constants compared with control (p values >0.5), and no experimental condition was acutely cytotoxic (Figure 4B). These results demonstrate that cells exposed to SWCNTs-BSA are able to grow and divide normally.

To determine cellular recovery from SWCNTs-BSA exposure, we monitored both the cellular expulsion of SWCNTs-BSA into the media and the cellular retention of SWCNTs-BSA as a function of time and original SWCNTs-BSA concentration. After passage and 1 h of fresh, SWCNT-free media, the SWCNTs-BSA retained per cell were moderately reduced and remained on the order of pg cell^{-1} (Figure 4C). Correspondingly, at 1 h the concentration of SWCNTs-BSA in the media normalized per cell was large (Figure 4D). In general, the data showed two distinct time periods of recovery. Immediately after passage (0 h), the cells began to adhere to the substrate and spread but were not proliferating. After 7 h (and before 24 h), cells began to proliferate.[50,51] In this temporal regime, it was likely that some cells were unable to adhere and spread after passage and died, releasing SWCNTs-BSA into the media. Also, since the media initially contained no SWCNTs-BSA, membrane-associated SWCNTs-BSA may have detached into the media. Hence, there was a slight increase in the concentration of SWCNTs-BSA in the media until the 7 h time point. Concomitantly, as the concentration of SWCNTs-BSA increased slightly in the media, healthy cells performing normal, active

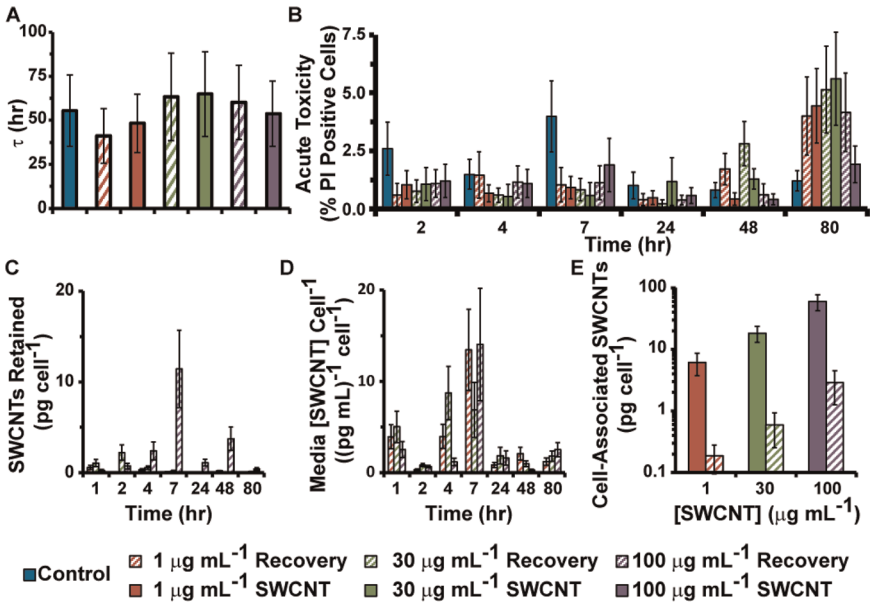

Figure 4. Recovery of cells from exposure to SWCNTs-BSA. (a) Cells seeded at standard density (3.0×10^4 cells cm^{-2}), exposed to SWCNTs-BSA, and allowed to recover showed no change in proliferation compared to control cells, as did those perpetually exposed to SWCNTs-BSA. (b) Acute toxicity was monitored at each time point after subculture, and no experimental condition was acutely cytotoxic. (c) The mass of SWCNTs-BSA remaining in cells that were allowed to recover was monitored as a function of time. The amount of SWCNTs per cell was minimal at long time. (d) The concentration of SWCNTs-BSA in the recovery media normalized by the amount of cells was quantified as a function of time. Initially, the concentration was relatively high and at long time was lower on a per cell basis. (e) The amount of SWCNTs per cell was significantly reduced for all recovery conditions compared to continually exposed cells, averaged over time (Student's *t* test, $p < 0.005$).

cellular processes may have internalized some of these extra expelled SWCNTs, increasing their net internalized SWCNTs-BSA concentration, since the rate of internalization is much faster than rate of recovery. Therefore, the concentration of SWCNTs-BSA both in the cells and in the media slightly increased until ~7 h.

After 24 h, cells have proliferated since they have a proliferation time constant of ~55 h. With substantially more cells and a finite amount of SWCNTs-BSA, the available SWCNTs-BSA per cell greatly decreased. While cells may stochastically internalize some SWCNTs-BSA from the media, the quantity internalized would be drastically reduced as the amount of SWCNTs-BSA in the media per cell would exponentially become smaller due to cell proliferation. This extracellular SWCNT condition would also be true for cells *in vivo*, with blood flow making the effective extracellular SWCNT concentration ~0. After 80 h, cells have proliferated by >300% from passage, and the concentration of SWCNTs-BSA in cells is ~0. In general, average SWCNTs-BSA uptake was statistically (*p* values <0.005) greater for perpetually exposed cells than that retained in recovery cells across all times (Figure 4e): recovery cells had ~3% the amount of SWCNTs as did cells with continual exposure to SWCNTs. Hence, NIH-3T3 cells are able to recover from SWCNTs-BSA exposure.

To determine a rate of recovery, the concentration of SWCNTs-BSA per cell was modeled using an exponential decay, beginning at the time of maximal internalized SWCNTs-BSA. The rates of recovery are 42 ± 19, 24 ± 10, and 28 ± 6 h^{-1} for 1, 30, and 100 μg mL^{-1}, respectfully. Thus, the rate of recovery was independent of original SWCNTs-BSA concentration—the average is 31 ± 7 h^{-1}—and was much slower than the extremely fast steady state reached for internalization at ~1 min. This recovery time constant is somewhat dependent on cell passage, and the fluctuations observed at 7 h may not be observed in nonpassaged cells. However, for SWCNT therapies that utilize preseeding of cells with SWCNTs and then systemic delivery of SWCNT−cells, passage-related changes will be relevant.

Imaging SWCNTs-BSA Recovery. To visualize cell recovery from SWCNTs-BSA, we performed confocal Raman spectroscopy and imaging co-registered to phase contrast microscopy and imaging (Figure 5 and larger views in Supporting Information, Figures 4−9). The SWCNT G-band, due to its intense and unique signal, was used to probe SWCNT local concentration by relating Raman G-band intensity to SWCNT concentration through a calibration curve (Supporting Information, Figure 1B). The SWCNT signal inside cells was substantially higher than external concentration, suggesting subcellular concentration of SWCNTs. Imaging revealed that SWCNTs were primarily located outside of the nucleus with a substantial peri-nuclear localization, previously reported by our group[4,7] and others.[36−38] The presence of peri-nuclear SWCNTs measured in a plane where the NIH-3T3 nucleus was in best focus suggests

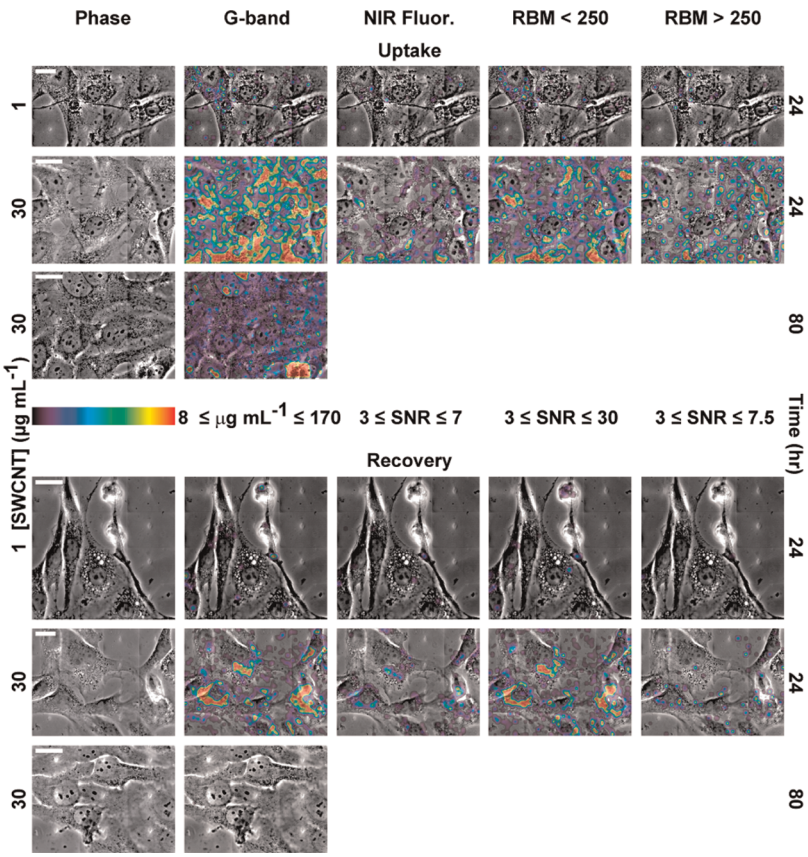

Figure 5. Confocal Raman imaging of fixed cells. Large fields of view were acquired by concatenating multiple fields of view (WiRE software). Confocal Raman mapping was performed, focusing on the G-band, the radial breathing mode (RBM), and the fluorescence peak. By using a standard curve relating concentration to G-band intensity, the subcellular, local concentration of SWCNTs-BSA was determined and is represented as color in the G-band maps. The SWCNTs-BSA fluorescence was relatively intense, confirming that cells did not alter the initial SWCNTs-BSA fluorescence. Analysis of the RBM recapitulated that, while cells process SWCNTs into locally high concentrations, SWCNTs-BSA remain individually dispersed (high RBM signal below 250 cm^{-1}). Scale bar is 20 μm.

that confocal Raman slices were taken within the cell and signal was not from outside the cell.

We have also collected SWCNT NIR fluorescence with the Raman spectra (Figure 5). Preservation of NIR fluorescence inside cells confirmed that SWCNTs were mostly intact. In some small regions with an absence of detectable fluorescence, either SWCNTs may have been in acidic vesicles leading to protonation and loss of fluorescence[54] or smaller concentrations of SWCNTs failed to produce a detectable fluorescence signal. We investigated the radial breathing modes (RBM) of the spectra,[55,56] wherein intensity above 250 cm^{-1} generally indicates SWCNT bundling, while intensity below 250 cm^{-1} is primarily from individual SWCNTs.[15,55] Confocal Raman spectra showed substantially more intensity (~350%) from the RBM < 250 cm^{-1} compared to the RBM > 250 cm^{-1}, suggesting little if any SWCNT bundling.

Potential Application: Cells As SWCNT Delivery Vehicles. A possible strategy to deliver SWCNTs locally within the body would be to preload cells with SWCNTs-BSA *in vitro* and use cells as vectors to deliver SWCNTs-BSA to other cells. To create such a delivery system, the rate parameters determined in this study are crucial for controlling the delivery time and quantity of SWCNTs-BSA. For example, NIH-3T3 cells could be loaded to 18 pg cell^{-1} by incubation with a 30 μg mL^{-1} solution of SWCNTs-BSA for 24 h. Our data suggest that other cell types, such as human mesenchymal stem cells, can take up larger amounts of SWCNTs-BSA.[7] Cells could be delivered to tissues (1:1 SWCNT-treated cells: endogenous cells). After ~60 h (~2 recovery rate time constants), the vector cells would fully expel their SWCNTs-BSA, generating a local extracellular concentration of ~0.35 μg mL^{-1}. This extracellular concentration would subsequently lead to ~0.15 pg cell^{-1} internalized by the target cells.

SUMMARY

Development of SWCNT-based biomedical technologies requires a quantitative understanding of uptake, biocompatibility, subcellular localization, and retention. Previous studies have typically only investigated uptake at a single and very low concentration (*e.g.*, ~1 μg mL^{-1}) or time point (*e.g.*, ~1 h).[19−21] Here, we present a comprehensive analysis across a broad phase space,

enabling the determination of quantitative rates for time- and concentration-dependent uptake and revealing threshold values unable to be obtained without such a thorough investigation.

Further, few studies have investigated retention as well as recovery. Here, we have systematically examined recovery; cellular recovery from exposure to and release of SWCNTs is critical to the design of devices. We have shown that SWCNTs-BSA enter cells in seconds and are expelled from cells over hours and days. It is foreseeable that a systemic administration of SWCNTs-BSA could be used as a potential therapy, as healthy cells would be able to readily recover from SWCNTs-BSA administration.

A critical barrier to designing SWCNT-based subcellular technologies is the lack of a detailed understanding of time- and concentration-dependent uptake and recovery. To create a foundation of rates, we quantified time- and concentration-dependent uptake, biocompatibility, and recovery of NIH-3T3 cells exposed to SWCNTs-BSA, providing critical design parameters for SWCNT-based biotechnologies. Additionally, we demonstrated the ability of cells to recover from SWCNTs, suggesting that SWCNTs-BSA can be utilized as a safe subcellular nanobiomaterial.

MATERIALS AND METHODS

SWCNTs-BSA Dispersion. SWCNTs-BSA were prepared as described previously.[3,5−7,57] The final product was highly purified, pristine, length-selected (145 ± 17 nm) HiPCO SWCNTs (diameter 1.0 ± 0.3 nm). Details about SWCNT preparation are also included in the Supporting Information.

SWCNTs-BSA Characterization. SWCNTs-BSA sample yield and qualitative dispersion quality were assessed using vis−NIR absorbance spectroscopy (Varian Cary 5000 UV−vis−NIR spectrophotometer) (Supporting Information, Figure 10A). SWCNT concentration was determined by an extinction coefficient of 2.6 absorbance mL mg^{-1} mm^{-1} at 930 nm.[58] The peaks of the spectrum arise from van Hove singularities of the density of states and qualitatively indicate dispersion quality.

To better verify SWCNT dispersion quality, we measured NIR fluorescence spectra from SWCNTs-BSA (Horiba Jobin Yvon Nanolog spectrofluorometer) (Supporting Information, Figure 10B). To this end, SWCNTs-BSA were diluted to 0.3 absorbance cm^{-1}, and NIR spectra were acquired for 60 s of exposure time with excitation and emission slit widths of 10 nm by a liquid-nitrogen-cooled Symphony InGaAs-1700 detector. The data were analyzed with Nanosizer software (Horiba Jobin Yvon). Numerous chiralities were observed, with minimal exciton energy transfer, indicating individually dispersed SWCNTs.[54]

We collected Raman spectra from SWCNTs-BSA dispersions using an inVia confocal Raman microscope (Renishaw; Supporting Information, Figure 10C) with a 785 nm laser (100 mW). The radial breath modes are characteristic of SWCNTs,[38,56] and intensity above 250 cm^{-1} generally indicates SWCNT bundling, while intensity below 250 cm^{-1} is primarily from individual SWCNTs.[38,56] The majority (∼85%) of RBM were <250 cm^{-1}, confirming SWCNTs were individually dispersed in suspension (left inset).[56,59] The laser also caused the SWCNTs to fluoresce, which was detected by the Raman system in the range of 2242 and 2649 cm^{-1} (right inset real-space wavelength).[38,55,56]

Cell Culture. NIH-3T3 cells were cultured in Dulbecco's modified Eagle's medium (DMEM with high glucose (4500 mg L^{-1}), with 4.0 mM L-glutamine, without sodium pyruvate, Thermo Scientific Hyclone) supplemented with 10% v/v newborn calf serum (Invitrogen) and 1% v/v streptomycin−penicillin (Invitrogen). Cells were maintained at 37 °C at 5% CO_2.

Determination of Uptake. For uptake studies, NIH-3T3 cells were passed into 6- or 96-well plates at a seeding density of 3×10^4 cells cm^{-2} and allowed to incubate for 24 h. Then, SWCNTs-BSA were added and diluted in cell culture media to their respective final concentrations. To ensure cellular effects were not mediated by different volumes of SWCNTs-BSA differently diluting the cell culture media, appropriate volumes of 1 wt % BSA in ultrapure water were added to the samples at lower SWCNTs-BSA concentration to maintain the same total volume of solution added.

After the indicated time of incubation with SWCNTs-BSA, the media was aspirated completely. "Wash step" cells received a wash with cell culture phosphate-buffered saline (Invitrogen), while "no wash step" did not. Cells were then maintained in cell culture PBS and rapidly imaged at 20× using phase contrast microscopy to enable a determination of cell count. A finite number of images ($n > 5$ of ∼0.4 mm^2 fields of view) were acquired, the cells were manually counted, and the total cells per well was calculated by extrapolating the average counts to the entire size of the well. Immediately after imaging, the cells were subjected to cell lysis buffer (Cell Signaling Technology), diluted to 1× in the cells' current PBS. After the addition of buffer, the cells were placed at 4 °C to aid the efficacy of the lysis buffer (manufacturer's recommendation), which also facilitated cell detachment from the substrate. The wells were also exposed to probe tip sonication for ∼5 s at 60 W to ensure complete cell lysis and to ensure that the SWCNTs were homogeneously distributed throughout the solution. Before acquiring data, the wells were again imaged using phase contrast microscopy to verify that cells were completely detached from the substrate.

To determine the concentration of SWCNTs in the cell lysis samples, the solutions were pipetted into a 24-well, glass (#1.5) bottom dish (MatTek) and subjected to confocal Raman spectroscopy. A Raman spectroscopy calibration curve ($R^2 = 0.998$) of G-band counts *versus* SWCNT concentration over multiple decades (initial sample concentration was determined *via* vis−NIR absorption spectroscopy and subjected to serial dilution) was developed and used to determine the concentration of SWCNTs from the cell lysates solutions' G-band signals (Supporting Information, Figure 1A). To ensure precise Raman G-band counts across multiple days, the system was precisely tuned to the same silicon standard before each experiment.

Determination of Proliferation and Viability. For biocompatibility studies, NIH-3T3 cells were passed into six-well plates at a seeding density of 1.5×10^4 cells cm^{-2} as the low density condition and 3.0×10^4 cells cm^{-2} as the standard seeding density.[50] Cells were incubated for 24 h and were then subjected to SWCNTs-BSA, as described above. After 48 h, the media was aspirated, the cells were washed with PBS, fresh media (− phenol red to enable imaging) was added, and the cells were exposed to Hoechst 33342 (Invitrogen, a cell-permeable nucleic acid stain and marker of all cells) at 10 μg mL^{-1} and propidium iodine (PI, Invitrogen, a cell-impermeable nucleic acid stain and marker of dead cells) at 500 nM for 15 min. The cells were rapidly imaged on a Leica DMI 6000B inverted light and fluorescence microscope maintained at 37 °C at 20× for blue (Hoechst 33342) fluorescence, red (PI) fluorescence, and phase contrast ($n > 10$ per well). Fluorescently labeled nuclei were automatically counted using ImageJ and were manually verified. For each condition, ∼1000 cells were analyzed.

Recovery. NIH-3T3 cells were passed into four separate dishes at 6×10^4 cells cm^{-2}. After 8 h, the cells were attached, and the dishes were subjected to the appropriate SWCNT condition: specifically, 0 (control), 1, 30, or 100 μg mL^{-1} of SWCNTs-BSA. After an additional 16 h, each dish was

concomitantly subcultured. To investigate time- and concentration-dependent recovery, cells were seeded into 96-well plates such that each time point had its own plate consisting of control, SWCNTs-BSA (1, 30, and 100 μg mL^{-1}), and recovery (1, 30, and 100 μg mL^{-1}) cells. Recovery cells for this study were cells that were exposed to SWCNTs-BSA before subculturing but were subsequently cultured in fresh, SWCNTs-BSA-free media after passing. For each point in the phase space (time, SWCNTs-BSA concentration, and recovery or perpetual SWCNT), samples were made for determining uptake and biocompatibility as described above.

Confocal Raman Spectroscopy and Imaging. Cell samples for confocal Raman imaging were prepared by culturing cells on sterilized #1.5 coverslips (Fisher) and subsequently fixing them in 3.7% formaldehyde (Sigma-Aldrich). Phase contrast and confocal Raman imaging were performed on an inverted Raman confocal microscope (inVia Raman microscope, Renishaw) with a 785 nm laser (100 mW), a 100× (1.4 NA) oil immersion phase objective (Leica Microsystems), and a 0.9 NA air condenser (Leica Microsystems) for phase-contrast imaging, as previously reported by our group.[7] The in-plane ($x-y$) resolution of the Raman microscope with the 100× objective is ~250 nm, and the z resolution is ~300 nm. For determining SWCNT uptake, the cell lysate solutions in the 24-well glass bottom dish were imaged using a 50× (0.75 NA) dry objective.

Control of mapping parameters and imaging processing were performed using WiRE software (Renishaw). Confocal Raman spectra were collected in a rectangular grid with step sizes of ≤2.50 μm. The G-band, centered at 1590 cm^{-1}, is indicative of SWCNTs.[38,55] To map G-band intensity, confocal Raman spectra between 1327 and 1819 cm^{-1} were collected with a 0.86 cm^{-1} resolution. The Raman signal-to-baseline at 1590 ± 17 cm^{-1} was analyzed in WiRE to obtain intensity maps of SWCNTs. Confocal Raman spectra between 100 and 715 cm^{-1} were collected with 1.07 cm^{-1} resolution, and signal-to-baseline intensity maps were made for the ranges 210−250 cm^{-1} (individual SWCNTs) and 250−280 cm^{-1} (bundled SWCNTs). Finally, to monitor SWCNT fluorescence,[38,55,56] confocal Raman spectra were collected between 2242 and 2649 cm^{-1} with 0.71 cm^{-1} resolution.

Modeling. SWCNTs-BSA cellular internalization was modeled based on a model and rate parameters developed by Jin *et al.*[19] The rate parameters used are as follows: $k_f = 1.2 \times 10^6$ M^{-1} s^{-1}; $k_r = 5.6 \times 10^{-3}$ s^{-1}; $k_e = 2.23 \times 10^{-4}$ s^{-1}; and $k_{rec} = 1.6 \times 10^{-5}$ s^{-1}, where k_f is the association rate constant of SWCNTs from the media with the cell membrane, k_r is the disassociation rate constant of SWCNTs from the media with the cell membrane, k_e is the rate constant of endocytosis, and k_{rec} is the rate constant of recycling. The equations were modeled in MATLAB (MathWorks) and solved using an ordinary differential equation solver capable of handling stiff equations (ode23tb), as the models' rapid equilibrium made for a stiff system.

Conflict of Interest: The authors declare no competing financial interest.

Acknowledgment. This work was supported by the NSF (CBET-0708418 and DMR-0619424 (K.N.D. and M.F.I.) and DMR-0645596 (M.F.I.)), the Sloan Foundation (M.F.I.), the Bertucci Graduate Fellowship (B.D.H.), and the National Defense Science and Engineering Graduate Fellowship (B.D.H.).

Supporting Information Available: Supporting text: detailed description of SWCNT preparation. Supporting figures: (1) Raman standard curves for SWCNT concentration; (2) representative images for proliferation and viability of cell seeding at low density; (3) representative images for proliferation and viability of cells seeded at "standard" density; (4−9) larger views of each of the experimental conditions of Figure 5; (10) spectroscopic assessment of SWCNTs-BSA quality. This material is available free of charge *via* the Internet at http://pubs.acs.org.

REFERENCES AND NOTES

1. Kolosnjaj, J.; Szwarc, H.; Moussa, F. Toxicity Studies of Carbon Nanotubes. In *Bio-Applications of Nanoparticles* Vol. 620; Chan, W. C. W., Ed.; Springer: New York, 2007; pp 181−204.
2. Liu, Z.; Tabakman, S.; Welsher, K.; Dai, H. Carbon Nanotubes in Biology and Medicine: *in Vitro* and *in Vivo* Detection, Imaging and Drug Delivery. *Nano Res.* **2009**, *2*, 85–120.
3. Holt, B. D.; Short, P. A.; Rape, A. D.; Wang, Y.-l.; Islam, M. F.; Dahl, K. N. Carbon Nanotubes Reorganize Actin Structures in Cells and *ex Vivo*. *ACS Nano* **2010**, *4*, 4872–4878.
4. Yaron, P.; Holt, B. D.; Short, P. A.; Losche, M.; Islam, M. F.; Dahl, K. N. Single Wall Carbon Nanotubes Enter Cells by Endocytosis and Not Membrane Penetration. *J. Nanobiotechnol.* **2011**, *9*, 45:1–45:15.
5. Islam, M. F.; Milkie, D. E.; Torrens, O. N.; Yodh, A. G.; Kikkawa, J. M. Magnetic Heterogeneity and Alignment of Single Wall Carbon Nanotubes. *Phys. Rev. B* **2005**, *71*, 037404(R): 1–037404(R):4.
6. Johnston, D. E.; Islam, M. F.; Yodh, A. G.; Johnson, A. T. Electronic Devices Based on Purified Carbon Nanotubes Grown by High-Pressure Decomposition of Carbon Monoxide. *Nat. Mater.* **2005**, *4*, 589–592.
7. Holt, B. D.; Dahl, K. N.; Islam, M. F. Quantification of Uptake and Localization of Bovine Serum Albumin-Stabilized Single-Wall Carbon Nanotubes in Different Human Cell Types. *Small* **2011**, *7*, 2348–2355.
8. Liu, Z.; Cai, W. B.; He, L. N.; Nakayama, N.; Chen, K.; Sun, X. M.; Chen, X. Y.; Dai, H. *In Vivo* Biodistribution and Highly Efficient Tumour Targeting of Carbon Nanotubes in Mice. *Nat. Nanotechnol.* **2007**, *2*, 47–52.
9. Liu, Z.; Sun, X. M.; Nakayama-Ratchford, N.; Dai, H. Supramolecular Chemistry on Water-Soluble Carbon Nanotubes for Drug Loading and Delivery. *ACS Nano* **2007**, *1*, 50–56.
10. Edri, E.; Regev, O. pH Effects on BSA-Dispersed Carbon Nanotubes Studied by Spectroscopy-Enhanced Composition Evaluation Techniques. *Anal. Chem.* **2008**, *80*, 4049–4054.
11. Edri, E.; Regev, O. "Shaken, Not Stable": Dispersion Mechanism and Dynamics of Protein-Dispersed Nanotubes Studied *via* Spectroscopy. *Langmuir* **2009**, *25*, 10459–10465.
12. Ge, C.; Du, J.; Zhao, L.; Wang, L.; Liu, Y.; Li, D.; Yang, Y.; Zhou, R.; Zhao, Y.; Chai, Z.; *et al*. Binding of Blood Proteins to Carbon Nanotubes Reduces Cytotoxicity. *Proc. Natl. Acad. Sci. U. S. A.* **2011**, *108*, 16968–16973.
13. Kam, N. W. S.; Dai, H. Carbon Nanotubes As Intracellular Protein Transporters: Generality and Biological Functionality. *J. Am. Chem. Soc.* **2005**, *127*, 6021–6026.
14. Kam, N. W. S.; Liu, Z. A.; Dai, H. Carbon Nanotubes As Intracellular Transporters for Proteins and DNA: An Investigation of the Uptake Mechanism and Pathway. *Angew. Chem., Int. Ed.* **2006**, *45*, 577–581.
15. Karajanagi, S. S.; Yang, H. C.; Asuri, P.; Sellitto, E.; Dordick, J. S.; Kane, R. S. Protein-Assisted Solubilization of Single-Walled Carbon Nanotubes. *Langmuir* **2006**, *22*, 1392–1395.
16. Lamprecht, C.; Liashkovich, I.; Neves, V.; Danzberger, J.; Heister, E.; Rangl, M.; Coley, H. M.; McFadden, J.; Fladaut, E.; Gruber, H. J.; *et al*. AFM Imaging of Functionalized Carbon Nanotubes on Biological Membranes. *Nanotechnology* **2009**, *20*, 434001.
17. Matsuura, K.; Saito, T.; Okazaki, T.; Ohshima, S.; Yumura, M.; Iijima, S. Selectivity of Water-Soluble Proteins in Single-Walled Carbon Nanotube Dispersions. *Chem. Phys. Lett.* **2006**, *429*, 497–502.
18. Nepal, D.; Geckeler, K. E. Proteins and Carbon Nanotubes: Close Encounter in Water. *Small* **2007**, *3*, 1259–1265.
19. Jin, H.; Heller, D. A.; Sharma, R.; Strano, M. S. Size-Dependent Cellular Uptake and Expulsion of Single-Walled Carbon Nanotubes: Single Particle Tracking and a Generic Uptake Model for Nanoparticles. *ACS Nano* **2009**, *3*, 149–158.
20. Jin, H.; Heller, D. A.; Strano, M. S. Single-Particle Tracking of Endocytosis and Exocytosis of Single-Walled Carbon Nanotubes in NIH-3T3 Cells. *Nano Lett.* **2008**, *8*, 1577–1585.
21. Cherukuri, P.; Bachilo, S. M.; Litovsky, S. H.; Weisman, R. B. Near-Infrared Fluorescence Microscopy of Single-Walled Carbon Nanotubes in Phagocytic Cells. *J. Am. Chem. Soc.* **2004**, *126*, 15638–15639.

22. Cherukuri, P.; Gannon, C. J.; Leeuw, T. K.; Schmidt, H. K.; Smalley, R. E.; Curley, S. A.; Weisman, R. B. Mammalian Pharmacokinetics of Carbon Nanotubes Using Intrinsic Near-Infrared Fluorescence. *Proc. Natl. Acad. Sci. U. S. A.* **2006**, *103*, 18882–18886.
23. Becker, M. L.; Fagan, J. A.; Gallant, N. D.; Bauer, B. J.; Bajpai, V.; Hobbie, E. K.; Lacerda, S. H.; Migler, K. B.; Jakupciak, J. P. Length-Dependent Uptake of DNA-Wrapped Single-Walled Carbon Nanotubes. *Adv. Mater.* **2007**, *19*, 939–945.
24. Feazell, R. P.; Nakayama-Ratchford, N.; Dai, H.; Lippard, S. J. Soluble Single-Walled Carbon Nanotubes As Longboat Delivery Systems for Platinum(IV) Anticancer Drug Design. *J. Am. Chem. Soc.* **2007**, *129*, 8438–8439.
25. Li, R. B.; Wu, R.; Zhao, L.; Wu, M. H.; Yang, L.; Zou, H. F. P-Glycoprotein Antibody Functionalized Carbon Nanotube Overcomes the Multidrug Resistance of Human Leukemia Cells. *ACS Nano* **2010**, *4*, 1399–1408.
26. Liu, Z.; Chen, K.; Davis, C.; Sherlock, S.; Cao, Q. Z.; Chen, X. Y.; Dai, H. Drug Delivery with Carbon Nanotubes for *in Vivo* Cancer Treatment. *Cancer Res.* **2008**, *68*, 6652–6660.
27. Tripisciano, C.; Kraemer, K.; Taylor, A.; Borowiak-Palen, E. Single-Wall Carbon Nanotubes Based Anticancer Drug Delivery System. *Chem. Phys. Lett.* **2009**, *478*, 200–205.
28. Wu, W.; Wieckowski, S.; Pastorin, G.; Benincasa, M.; Klumpp, C.; Briand, J. P.; Gennaro, R.; Prato, M.; Bianco, A. Targeted Delivery of Amphotericin B to Cells by Using Functionalized Carbon Nanotubes. *Angew. Chem., Int. Ed.* **2005**, *44*, 6358–6362.
29. Zhang, X. K.; Meng, L. J.; Lu, Q. H.; Fei, Z. F.; Dyson, P. J. Targeted Delivery and Controlled Release of Doxorubicin to Cancer Cells Using Modified Single Wall Carbon Nanotubes. *Biomaterials* **2009**, *30*, 6041–6047.
30. Herrero, M. A.; Toma, F. M.; Al-Jamal, K. T.; Kostarelos, K.; Bianco, A.; Da Ros, T.; Bano, F.; Casalis, L.; Scoles, G.; Prato, M. Synthesis and Characterization of a Carbon Nanotube-Dendron Series for Efficient siRNA Delivery. *J. Am. Chem. Soc.* **2009**, *131*, 9843–9848.
31. Lu, Q.; Moore, J. M.; Huang, G.; Mount, A. S.; Rao, A. M.; Larcom, L. L.; Ke, P. C. RNA Polymer Translocation with Single-Walled Carbon Nanotubes. *Nano Lett.* **2004**, *4*, 2473–2477.
32. Pantarotto, D.; Singh, R.; McCarthy, D.; Erhardt, M.; Briand, J. P.; Prato, M.; Kostarelos, K.; Bianco, A. Functionalized Carbon Nanotubes for Plasmid DNA Gene Delivery. *Angew. Chem., Int. Ed.* **2004**, *43*, 5242–5246.
33. Kam, N. W. S.; Jessop, T. C.; Wender, P. A.; Dai, H. Nanotube Molecular Transporters: Internalization of Carbon Nanotube-Protein Conjugates into Mammalian Cells. *J. Am. Chem. Soc.* **2004**, *126*, 6850–6851.
34. Strano, M. S.; Jin, H. Where Is It Heading? Single-Particle Tracking of Single-Walled Carbon Nanotubes. *ACS Nano* **2008**, *2*, 1749–1752.
35. Yehia, H.; Draper, R.; Mikoryak, C.; Walker, E.; Bajaj, P.; Musselman, I.; Daigrepont, M.; Dieckmann, G.; Pantano, P. Single-Walled Carbon Nanotube Interactions with HeLa Cells. *J. Nanobiotechnol.* **2007**, *5*, 8:1–8:17.
36. Albini, A.; Mussi, V.; Parodi, A.; Ventura, A.; Principi, E.; Tegami, S.; Rocchia, M.; Francheschi, E.; Sogno, I.; Cammarota, R.; *et al*. Interactions of Single-Wall Carbon Nanotubes with Endothelial Cells. *Nanomed.-Nanotechnol.* **2010**, *6*, 277–288.
37. Choi, J. H.; Nguyen, F. T.; Barone, P. W.; Heller, D. A.; Moll, A. E.; Patel, D.; Boppart, S. A.; Strano, M. S. Multimodal Biomedical Imaging with Asymmetric Single-Walled Carbon Nanotube/Iron Oxide Nanoparticle Complexes. *Nano Lett.* **2007**, *7*, 861–867.
38. Heller, D. A.; Baik, S.; Eurell, T. E.; Strano, M. S. Single-Walled Carbon Nanotube Spectroscopy in Live Cells: Towards Long-Term Labels and Optical Sensors. *Adv. Mater.* **2005**, *17*, 2793–2799.
39. Zhou, F. F.; Xing, D.; Wu, B. Y.; Wu, S. N.; Ou, Z. M.; Chen, W. R. New Insights of Transmembranal Mechanism and Subcellular Localization of Noncovalently Modified Single-Walled Carbon Nanotubes. *Nano Lett.* **2010**, *10*, 1677–1681.
40. Liu, Z. A.; Li, X. L.; Tabakman, S. M.; Jiang, K. L.; Fan, S. S.; Dai, H. Multiplexed Multicolor Raman Imaging of Live Cells with Isotopically Modified Single Walled Carbon Nanotubes. *J. Am. Chem. Soc.* **2008**, *130*, 13540–13541.
41. Welsher, K.; Liu, Z.; Sherlock, S. P.; Robinson, J. T.; Chen, Z.; Daranciang, D.; Dai, H. A Route to Brightly Fluorescent Carbon Nanotubes for Near-Infrared Imaging in Mice. *Nat. Nanotechnol.* **2009**, *4*, 773–780.
42. Ruggiero, A.; Villa, C. H.; Bander, E.; Rey, D. A.; Bergkvist, M.; Batt, C. A.; Manova-Todorova, K.; Deen, W. M.; Scheinberg, D. A.; McDevitt, M. R. Paradoxical Glomerular Filtration of Carbon Nanotubes. *Proc. Natl. Acad. Sci. U. S. A.* **2010**, *107*, 12369–12374.
43. Kam, N. W. S.; O'Connell, M.; Wisdom, J. A.; Dai, H. Carbon Nanotubes As Multifunctional Biological Transporters and Near-Infrared Agents for Selective Cancer Cell Destruction. *Proc. Natl. Acad. Sci. U. S. A.* **2005**, *102*, 11600–11605.
44. Kim, J.-W.; Kotagiri, N.; Kim, J.-H.; Deaton, R. *In Situ* Fluorescence Microscopy Visualization and Characterization of Nanometer-Scale Carbon Nanotubes Labeled with 1-Pyrenebutanoic Acid, Succinimidyl Ester. *Appl. Phys. Lett.* **2006**, *88*, 213110:1–213110:3.
45. Kostarelos, K.; Lacerda, L.; Pastorin, G.; Wu, W.; Wieckowski, S.; Luangsivilay, J.; Godefroy, S.; Pantarotto, D.; Briand, J. P.; Muller, S.; *et al*. Cellular Uptake of Functionalized Carbon Nanotubes Is Independent of Functional Group and Cell Type. *Nat. Nanotechnol.* **2007**, *2*, 108–113.
46. Lacerda, L.; Pastorin, G.; Gathercole, D.; Buddle, J.; Prato, M.; Bianco, A.; Kostarelos, K. Intracellular Trafficking of Carbon Nanotubes by Confocal Laser Scanning Microscopy. *Adv. Mater.* **2007**, *19*, 1480–1484.
47. Nakayama-Ratchford, N.; Bangsaruntip, S.; Sun, X.; Welsher, K.; Dai, H. Noncovalent Functionalization of Carbon Nanotubes by Fluorescein–Polyethylene Glycol: Supramolecular Conjugates with pH-Dependent Absorbance and Fluorescence. *J. Am. Chem. Soc.* **2007**, *129*, 2448–2449.
48. Nyquist, H. Certain Topics in Telegraph Transmission Theory. *P. IEEE* **2002**, *90*, 280–305.
49. Worle-Knirsch, J. M.; Pulskamp, K.; Krug, H. F. Oops They Did It Again! Carbon Nanotubes Hoax Scientists in Viability Assays. *Nano Lett.* **2006**, *6*, 1261–1268.
50. Todaro, G. J.; Green, H. Quantitative Studies of the Growth of Mouse Embryo Cells in Culture and Their Development into Established Lines. *J. Cell Biol.* **1963**, *17*, 299–313.
51. Vasiliev, J. M. Spreading of Non-Transformed and Transformed Cells. *Biochim. Biophys. Acta, Rev. Cancer* **1984**, *780*, 21–65.
52. Cui, D. X.; Tian, F. R.; Ozkan, C. S.; Wang, M.; Gao, H. J. Effect of Single Wall Carbon Nanotubes on Human HEK293 Cells. *Toxicol. Lett.* **2005**, *155*, 73–85.
53. Luoto, K.; Holopainen, M.; Perander, M.; Karppinen, K.; Savolainen, K. M. Cellular Effects of Particles-Impact of Dissolution on Toxicity of Man-Made Mineral Fibers. *Cent. Eur. J. Public Health* **1996**, *4*, 29–32.
54. O'Connell, M. J.; Bachilo, S. M.; Huffman, C. B.; Moore, V. C.; Strano, M. S.; Haroz, E. H.; Rialon, K. L.; Boul, P. J.; Noon, W. H.; Kittrell, C.; *et al*. Band Gap Fluorescence from Individual Single-Walled Carbon Nanotubes. *Science* **2002**, *297*, 593–596.
55. Dresselhaus, M. S.; Dresselhaus, G.; Saito, R.; Jorio, A. Raman Spectroscopy of Carbon Nanotubes. *Phys. Rep.* **2005**, *409*, 47–99.
56. Jorio, A.; Pimenta, M. A.; Filho, A. G. S.; Saito, R.; Dresselhaus, G.; Dresselhaus, M. S. Characterizing Carbon Nanotube Samples with Resonance Raman Scattering. *New J. Phys.* **2003**, *5*, 139.
57. Islam, M. F.; Rojas, E.; Bergey, D. M.; Johnson, A. T.; Yodh, A. G. High Weight Fraction Surfactant Solubilization of Single-Wall Carbon Nanotubes in Water. *Nano Lett.* **2003**, *3*, 269–273.
58. Fagan, J. A.; Becker, M. L.; Chun, J.; Hobbie, E. K. Length Fractionation of Carbon Nanotubes Using Centrifugation. *Adv. Mater.* **2008**, *20*, 1609–1613.

59. Schipper, M. L.; Nakayama-Ratchford, N.; Davis, C. R.; Kam, N. W. S.; Chu, P.; Liu, Z.; Sun, X.; Dai, H.; Gambhir, S. S. A Pilot Toxicology Study of Single-Walled Carbon Nanotubes in a Small Sample of Mice. *Nat. Nanotechnol.* **2008**, *3*, 216–221.